ResearchGate

See discussions, stats, and author profiles for this publication at: https://www.researchgate.net/publication/24277373

In situ gelation of P(NIPAM-HEMA) microgel dispersion and its applications as Injectable 3D cell scaffold

ARTICLE *in* BIOMACROMOLECULES · MAY 2009

Impact Factor: 5.75 · DOI: 10.1021/bm900022m · Source: PubMed

CITATIONS
50

READS
88

3 AUTHORS, INCLUDING:

Yongjun Zhang
Nankai University

89 PUBLICATIONS **1,785** CITATIONS

SEE PROFILE

Available from: Yongjun Zhang
Retrieved on: 02 February 2016

In Situ Gelation of P(NIPAM-HEMA) Microgel Dispersion and Its Applications as Injectable 3D Cell Scaffold

Tiantian Gan, Yongjun Zhang,* and Ying Guan

Key Laboratory of Functional Polymer Materials, Institute of Polymer Chemistry, College of Chemistry, Nankai University, Tianjin 300071, China

Received January 6, 2009; Revised Manuscript Received March 29, 2009

In this work we try to develop a new thermal gelling injectable scaffold for three-dimensional cell culture. Instead of using linear, branched, or grafted macromolecules, thermosensitive microgel particles or microspheres are used as building blocks for the construction of the macroscopic hydrogel scaffold. As a proof of concept, thermosensitive poly(*N*-isopropylacrylamide-*co*-2-hydroxyethyl methacrylate) (P(NIPAM-HEMA)) microgel particles were synthesized, which present a volume phase transition temperature (VPTT) at about 29 °C. Rheological test shows that the concentrated P(NIPAM-HEMA) microgel dispersion is colloidally stable when heated above its VPTT, indicating hydrophobic interaction alone can not induce thermal gelation of the dispersion. In the presence of a low concentration of $CaCl_2$, however, with the introduction of additional ionic cross-linking, the microgel dispersion gelates and forms macroscopic hydrogel. Gelation temperature of the microgel dispersion decreases with increasing ionic strength. SEM observation reveals that the resultant bulky gel has an interconnected porous microstructure. 293T cells, a human cell line, were encapsulated inside the hydrogel by simple mixing with the microgel dispersion at room temperature and heating to 37 °C. MTT (3-[4,5-dimethylthiazol-2-yl]-3,5-diphenyl tetrazolium bromide) assays reveal that the cells are viable and proliferate inside the 3D scaffold.

Introduction

Three-dimensional cell scaffolds, which mimic the natural extracellular matrices, play a key role in tissue engineering.[1] They also provide a promising tool for drug discovery[2] and the study of cell interactions.[3,4] The scaffolds can either be preformed with three-dimensional porous structure or an injectable one.[1] As for the preformed scaffolds, prior knowledge of the size and shape of the defect or cavity to be filled is necessary. Moreover, cell seeding can be inefficient due to poor transport of cells through the matrix and cellular damage. In contrast with the use of an injectable scaffold, because the scaffold forms in situ, it can fill a cavity with any size or shape. In addition, a more homogeneous distribution of bioactive molecules and cells within the matrices can readily be obtained. Because it does not require an invasive surgery for implantation, from a clinical perspective, the use of injectable scaffolds is very attractive as it minimizes patient discomfort, risk of infection, scar formation, and the cost of treatment.[5]

Many systems gelated in situ have been developed as injectable scaffolds.[5] Generally there are two types of injectable scaffolds, that is, chemically cross-linked and physically cross-linked. Chemically cross-linked scaffolds form by in situ polymerization induced either by heat or light or other in situ reactions between two components. However, toxic chemical agents are often employed in the formulations, adversely affecting cells and bioactive molecules during solidification. In contrast, physically cross-linked scaffolds form as a result of in situ gelation in response to certain environmental change. Therefore, they can overcome these limitations by avoiding the use of toxic agents.

Thermosensitive polymers are very attractive for use as injectable scaffolds.[6] When injected into the implant site and brought to body temperature, they gelate spontaneously and form a 3D scaffold in situ. The operation is quite convenient. No extra chemical agents are required, thus, their adverse effects are totally avoided. A lot of natural or seminatural polymers, including cellulose, chitosan, xyloglucan, gelatin, and their derivatives, and synthetic polymers, including polyethers, block copolymers of polyethers and polyesters,[7,8] and synthetic polypeptides, are thermosensitive.[9] Under appropriate conditions, they may gelate by heating, hence, hold great promise for the use as injectable scaffolds.

Up to now, to the best of our knowledge, all thermal gelling injectable scaffolds employ linear or branched thermosensitive polymers. Here we propose that, instead of linear or branched polymers, thermosensitive microgel particles or microspheres may be a better choice as building blocks for thermal gelling injectable scaffolds. Potential advantages of microgel particles over linear macromolecules include reduced viscosity and better mechanical properties at the same concentration. In addition, the use of microgel particles opens the possibility to encapsulate growth factors or other bioactive molecules in the interior of the particles and release them in proper time to guide the differentiation of stem cells.[10]

As a proof of concept, here we synthesized a thermosensitive poly(*N*-isopropylacrylamide-*co*-2-hydroxyethyl methacrylate) (P(NIPAM-HEMA)) microgel. We found that the microgel dispersion undergoes thermal gelation under proper conditions. Cells can be easily encapsulated in these in situ-formed bulky gels. Successful cell culture in these gels proved that these materials provide a proper environment for the proliferation of cells.

Experimental Section

Materials. *N*-Isopropylacrylamide (NIPAM), 2-hydroxyethyl methacrylate (HEMA), *N*,*N*′-methylenebis(acrylamide) (BIS), ammonium persulfate (APS), and sodium dodecyl sulfate (SDS) were purchased

* To whom correspondence should be addressed. E-mail: yongjunzhang@nankai.edu.cn.

10.1021/bm900022m CCC: $40.75 © 2009 American Chemical Society
Published on Web 04/14/2009

from Aldrich or Acros. NIPAM was purified by recrystallization from a hexane/acetone mixture and dried in a vacuum. HEMA was distilled under reduced pressure.

Microgel Synthesis. The P(NIPAM-HEMA) microgels were synthesized by free radical precipitation polymerization. NIPAM (0.792 g, 7 mmol), HEMA (0.391 g, 3 mmol), BIS (0.031 g, 0.2 mmol), and SDS (0.058 g, 0.2 mmol) were dissolved in 95 mL of water. The solution was filtered to remove any possible precipitates. The reaction mixture was transferred to a three-necked round-bottom flask equipped with a condenser and a nitrogen inlet and heated to 70 °C under a gentle stream of nitrogen. After 1 h, 0.068 g of APS (dissolved in 5 mL of water) was added to initiate the reaction. The reaction was allowed to proceed for 5 h. The resultant microgels were purified by dialysis (cutoff 12000−14000 Da) against water with frequent water change for at least 1 week.

Microgel Particle Size. The size of the microgel particles were measured by dynamic light scattering with a Brookhaven 90Plus laser particle size analyzer. All the measurements were carried out at a scattering angle of 90°. The sample temperature was controlled with a built-in Peltier temperature controller.

Rheological Characterization. The purified microgel dispersion was concentrated by evaporating at 60 °C. An aliquot of the dispersion was dried at 120 °C. The concentration of the concentrated dispersion was calculated from the weight difference induced by the drying process. Dynamic rheological analysis of the concentrated dispersions was performed on an AR2000ex rheometer (TA Instruments). Aluminum parallel plate geometry with a diameter of 40 mm was used. The sample gap was set to be 1.0 mm. The temperature was controlled by a Peltier system in the bottom plate connected with a water bath. Temperature-dependent changes in elastic (storage) modulus, G', and viscous (loss) modulus, G'', were recorded in a dynamic temperature ramp test (DTRT). All the rheological experiments were performed within the linear viscoelastic region.

SEM. SEM images were recorded on a SHIMADZU Superscan SS-550 scanning electron microscope. The samples were sputter-coated with PdAu before the imaging.

Cell Culture. A total of 5 mL of 293T cell dispersion with a concentration of about 1×10^5 cells/mL was mixed with 5 mL of 6 wt % microgel dispersion containing 0.005 M $CaCl_2$ and 0.137 M NaCl. The mixture was brought to 37 °C and gelated immediately. It was cut into round disks with a diameter of 4 mm and a height of 3 mm using a cork borer. The cells were cultured in a media containing 90% Dulbecco's modified Eagle medium (DMEM), 10% heat-inactivated fetal calf serum, and 100 units/mL of penicillin/streptomycin. The cultures were maintained in an incubator at 37 °C with a humidified atmosphere of 5% CO_2. The medium was changed every 2−3 days.

MTT Assay. The cell proliferation was measured using MTT assay. After cultured for a predeterminated period, the cells were incubated with 2 mL of MTT solution (5 mg/mL) for 12 h at 37 °C. Then 10 mL of DMSO were added to dissolve the resultant formazan crystals. The UV absorbance of the solubilized formazan crystals was measured spectrophotometrically at 490 nm to determine the number of living cells.

Cell Morphology. The appearance of the cells cultured in the scaffold was observed in situ by Olympus LX70-140 inverted fluorescence microscope at room temperature. The samples were stained with acridine orange (AO) before imaging. The excitation wavelength used for AO was 450 ± 20 nm.

Results and Discussion

Poly(*N*-isopropylacrylamide) (PNIPAM) is a well-known thermosensitive polymer. At a temperature below its lower critical solution temperature (LCST), it is hydrophilic and soluble in water, however, it collapses and precipitates from water when heating above its LCST. Under appropriate conditions, it thermally gelates and forms a physical hydrogel. Loosely cross-linked PNIPAM hydrogel and copolymer hydrogel of NIPAM and acrylic acid were first synthesized and tested as injectable cell scaffold in 1999.[11,12] Later linear copolymer of NIPAM with ionic comonomers[13] and PNIPAM-grafted gelatin[14] and hyaluronan[15] have also been developed as injectable scaffolds. These previous researches show that the PNIPAM polymers are not cytotoxic and have potential use as cell culture substrate and cell delivery vehicles.[13] The thermal gelation of PNIPAM polymers is attributed to the hydrophobic interaction among the shrunk PNIPAM chains. At a relatively high concentration, the dehydrated PNIPAM chains associate through intermolecular hydrophobic interaction and form physical cross-links, resulting in the thermal gelation of the solution.[14]

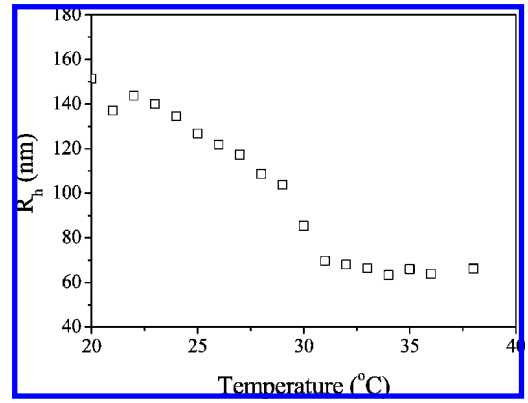

Figure 1. Hydrodynamic radii of P(NIPAM-HEMA) microgels measured at various temperatures.

In this contribution, however, we synthesized thermosensitive PNIPAM microgels and used them as injectable scaffold for cell culture. Because polymers from 2-hydroxyethyl methacrylate (HEMA) have been widely used as biomaterials because of their good biocompatibility,[16,17] it was selected as a comonomer to synthesize a copolymer microgel with NIPAM. Although the P(NIPAM-HEMA) microgels have a high HEMA content (about 30 mol % from the feed ratio), they still present a thermosensitive swelling behavior, as shown in Figure 1. The hydrodynamic radii (R_h) of the microgel particles decrease with increasing temperature. Compared with pure PNIPAM microgels, which present a sharp decrease in R_h at the volume phase transition temperature (VPTT) (corresponding to LCST of the linear polymer), the phase transition of P(NIPAM-HEMA) microgels is rather smooth. A similar result has been observed by Brugger and Richtering and was attributed to the high content of HEMA comonomer in the microgels.[18] The VPTT of the P(NIPAM-HEMA) microgels was determined to be 29 °C, where the shrinking of the particle accelerates, which is about 3 °C lower than that of the pure PNIPAM microgels (about 32 °C). Other authors have also reported that the incorporation of HEMA slightly shift the VPTT of the copolymer microgels to a lower temperature.[19] The lower VPTT of P(NIPAM-HEMA) microgels can be attributed to the hydrogen-bonding between the hydroxyl groups in HEMA and amide groups in NIPAM, which makes the copolymer microgels more hydrophobic.

In the absence of added salt, the PNIPAM-based microgel dispersions are highly stable even at a temperature much higher than its LCST. They may flocculate when heated above their LCST in an electrolyte solution, however, the flocculation is reversible as the resulting flocs redisperse when cooled back to room temperature.[20] Macroscopic hydrogels formed from PNIPAM-based microgel dispersions have been reported in the literature, however, these microgels either have a special

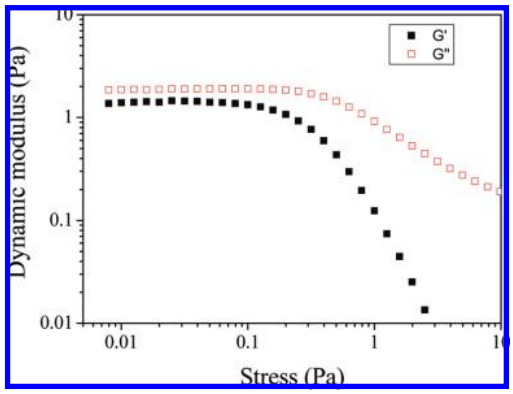

Figure 2. Storage and loss moduli (G' and G'') of a P(NIPAM-HEMA) microgel dispersion as a function of stress applied at 10 °C and a frequency of 0.1 Hz. The polymer concentration of the dispersion is 6.0 wt %.

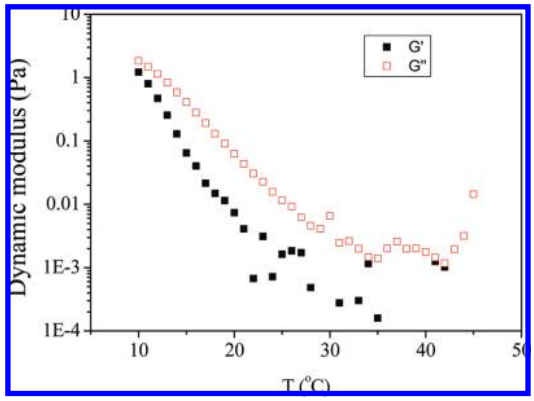

Figure 3. Evolution of the dynamic modulus of P(NIPAM-HEMA) microgels with temperature increases under 0.05 Pa and 0.1 Hz. The polymer concentration of the dispersion is 6.0 wt %.

interpenetrated network[21] or are copolymerized with a special comonomer.[22] Here we report that common PNIPAM microgel dispersions may gelate thermally and form macroscopic hydrogels, which are stable under physiological conditions.

To study the thermal gelation of the P(NIPAM-HEMA) microgel dispersions, the dispersions were first concentrated. Their rheological properties were measured under various conditions. Stress sweep experiments at a frequency of 0.1 Hz were first carried out to define the linear viscoelastic region. As shown in Figure 2, there is no significant change in storage and loss modulus, G' and G'', below a stress of 0.1 Pa. To ensure that the rheological measurements were performed within linear viscoelastic region, all measurements thereafter were performed at a stress of 0.1 Pa and a frequency of 0.1 Hz.

Figure 3 shows the evolution of the storage and loss moduli G' and G'' of the concentrated microgel dispersion as temperature increases. Over the entire temperature range studied, G'' is always larger than G', indicating that the dispersion remains in a liquid state. In addition, both G' and G'' decrease with the increasing temperature. This phenomenon was first reported by Senff and Richtering[23] and later also by other authors. As the temperature increases, the microgel particles shrink gradually, resulting in a decreased effective volume fraction of the particles and, in turn, decreased viscosity and elastic properties. When the temperature is higher than 31 °C, the size of the microgel particle stops reducing, as evidenced by Figure 1. Both G' and G'' stop decreasing, however, a strong fluctuation in G' was observed because its value is rather low, which makes an accurate measurement difficult. These results indicate that the concentrated microgel dispersion keeps colloidally stable even at a temperature well above its VPTT.

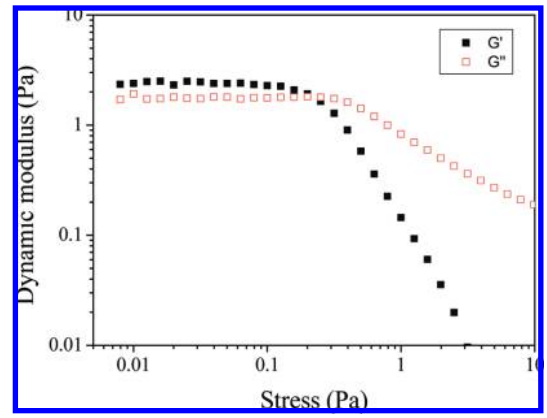

Figure 4. Storage and loss moduli (G' and G'') of a P(NIPAM-HEMA) microgel dispersion as function of stress applied in the presence of 0.005 M $CaCl_2$. T = 10 °C. Oscillation frequency is 0.1 Hz. The polymer concentration of the dispersion is 6.0 wt %.

The interactions among the microgel particles include van der Waals attraction, electrostatic interaction, and steric interaction.[24] Because APS was used as initiator, negatively charged groups are incorporated on the surface of the microgel particles during polymerization. The electrostatic repulsion among the particles helps to keep the dispersion stable. At a low temperature, the particles are hydrophilic and highly swollen. The van der Waals attraction among them is negligible, therefore, the microgel dispersion is intrinsically stable to flocculation. Upon heating, the microgel particles become hydrophobic gradually, resulting in increased van der Waals attraction. However, the result shown in Figure 3 indicates that the electrostatic repulsion dominates van der Waals attraction and the dispersion keeps stable at a temperature well above its VPTT.

Figure 4 shows the stress dependence of G' and G'' of the concentrated microgel dispersion in the presence of 0.005 M $CaCl_2$ at 10 °C. In this case, the storage modulus G' is larger than the loss modulus G'', that is, the dispersion behaves more like a solid, suggesting the formation of a physical network. In contrast, in the absence of $CaCl_2$, the dispersion behaves more like a liquid (Figure 2). The formation of a physical network should be attributed to the ionic cross-linking of the microgel particles with Ca^{2+}. As we mentioned above, the surface of the microgel particles bears negative charges, which originates from the APS initiator. As a bivalent cation, Ca^{2+} can ionically bond with two microgel particles simultaneously. Hence, an ionically bonded network of the microgel particles forms in the microgel dispersion. It is well-known that Ca^{2+} can ionically cross-link alginate[25] and proteins to form hydrogels. Figure 4 also shows that both G' and G'' do not change when stress is below 0.1 Pa, which can be defined as linear viscoelastic region for this system. The physical network can be destroyed by higher stress. A crossover of G' and G'' was observed at a stress of 0.2 Pa. Beyond this point, G'' is larger than G', indicating the physical network is destroyed by the applied stress and the hydrogel is liquidated.

The evolution of the dynamic modulus G' and G'' of the concentrated microgel dispersion in the presence of Ca^{2+} was measured through a temperature ramp. As shown in Figure 5, both G' and G'' decrease with increasing temperature, which has been attributed to the shrinking of the microgel particles. However, when the temperature approaches the VPTT of the microgels, both G' and G'' increase sharply. A crossover of G'

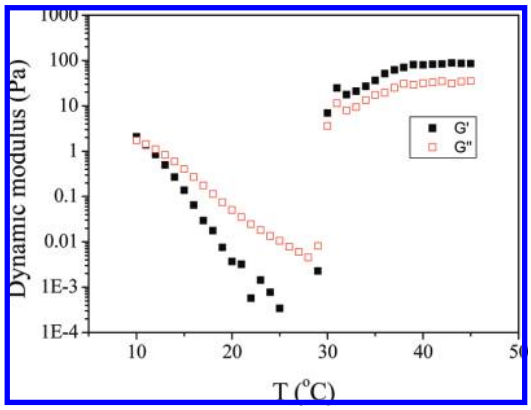

Figure 5. Evolution of dynamic modulus of the P(NIPAM-HEMA) microgel dispersion with temperature increase in the presence of 0.005 M $CaCl_2$ under a stress of 0.05 Pa and a frequency of 0.1 Hz. The polymer concentration of the dispersion is 6.0 wt %.

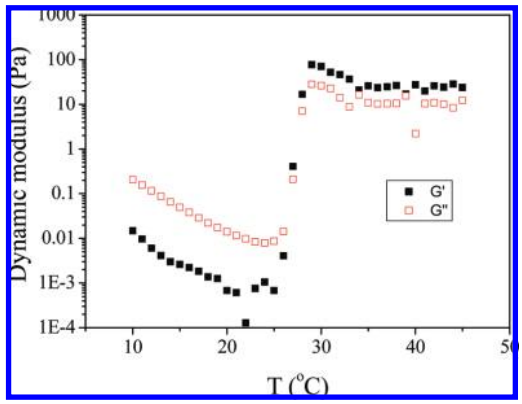

Figure 6. Evolution of dynamic modulus of P(NIPAM-HEMA) microgel dispersion with temperature increase at 0.05 Pa and 0.1 Hz. The concentrations of the P(NIPAM-HEMA) polymer, $CaCl_2$ and NaCl are 6.0 wt %, 0.005 M and 0.137 M, respectively.

and G'' was observed at about 29.5 °C. At a temperature higher than this point, G' is always larger than G'', indicating the formation of a physical network.

The result shown in Figure 5 clearly indicates the thermal gelation of the concentrated microgel dispersion. A lot of methods have been proposed to define the gelation point. The simplest method is to define the point where G' and G'' crossover as gelation point. According to this method, the gelation temperature of this system is determined to be 29.5 °C, which is close to the VPTT of the microgels. This fact suggests that the hydrophobic interaction between the collapsed microgel particles plays a major role for the gelation of the dispersion. In contrast, Figure 3 shows that the same dispersion does not gelate in the absence of Ca^{2+}. These results indicate that hydrophobic interaction alone can not result in the thermal gelation of the dispersion. However, in the presence of $CaCl_2$, with the additional ionic cross-linking of the microgel particles, the physical network of microgel particles can form and the dispersion can gelate.

As our purpose is to develop injectable 3D cell scaffold, besides $CaCl_2$, some NaCl was added to the microgel dispersion to achieve a physiologic ionic strength. The thermal gelation of the dispersion was also studied using the same conditions. As shown in Figure 6, again we observed a sharp increase in both G' and G'' when temperatures approach VPTT of the microgels. G' and G'' crossover at 27 °C, which was defined as gelation temperature for this system. Compared with the result in Figure 5, a 2.5 °C shift toward low temperature in gelation

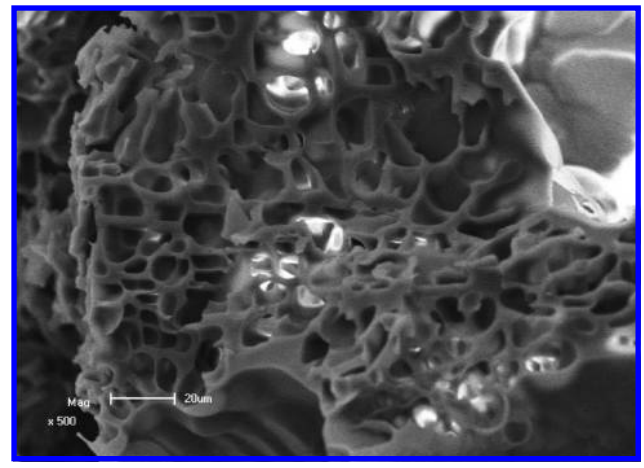

Figure 7. SEM image of the cross section of the thermally gelated macroscopic hydrogel.

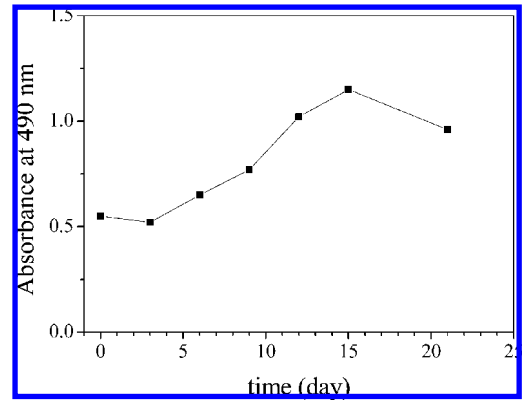

Figure 8. Proliferation of 293T cells cultured in the in situ formed P(NIPAM-HEMA) microgel scaffold as assessed by MTT assays.

temperature was observed in the presence of NaCl. The shift of gelation temperature is in line with the decease in VPTT of PNIPAM microgels at a higher ionic strength.[20,26] This effect has been attributed to the competing interactions between salt and water and between water and polymer chains.[27] The relationship between gelation temperature and VPTT reveals that the gelation of the dispersion should again be attributed to the hydrophobic interaction among the shrunk microgel particles. Besides the ionic cross-linking of Ca^{2+}, the screening of electrostatic repulsion by NaCl is also beneficial for the gelation of the dispersion. In fact, in a control experiment, the microgel dispersion added with 0.154 M NaCl gelates too, indicating the electrostatic repulsion is efficiently screened by the high ionic strength (see Figure 1 in Supporting Information).

To investigate the microstructure of the resultant hydrogel, the concentrated microgel dispersion was gelated by heating to 37 °C. The resultant gel was quickly frozen in liquid nitrogen and dried under vacuum. We assume the delicate microstructure of the sample can be conserved and the cross section, as observed using SEM, reveals the interior structure of the hydrogel. As shown in Figure 7, the gel presents an interconnected porous structure with pore size ranging from several to several tens of microns. This interconnected porous microstructure is believed to be beneficial for cell culture because it allows for cell migration and transport of nutrients and waste products in and out of the scaffold. The microstructure revealed by SEM is critically depended on the freezing/drying procedure. When the freezing was not quick enough, densely packed structure was observed, as this procedure allowed for the reswelling and

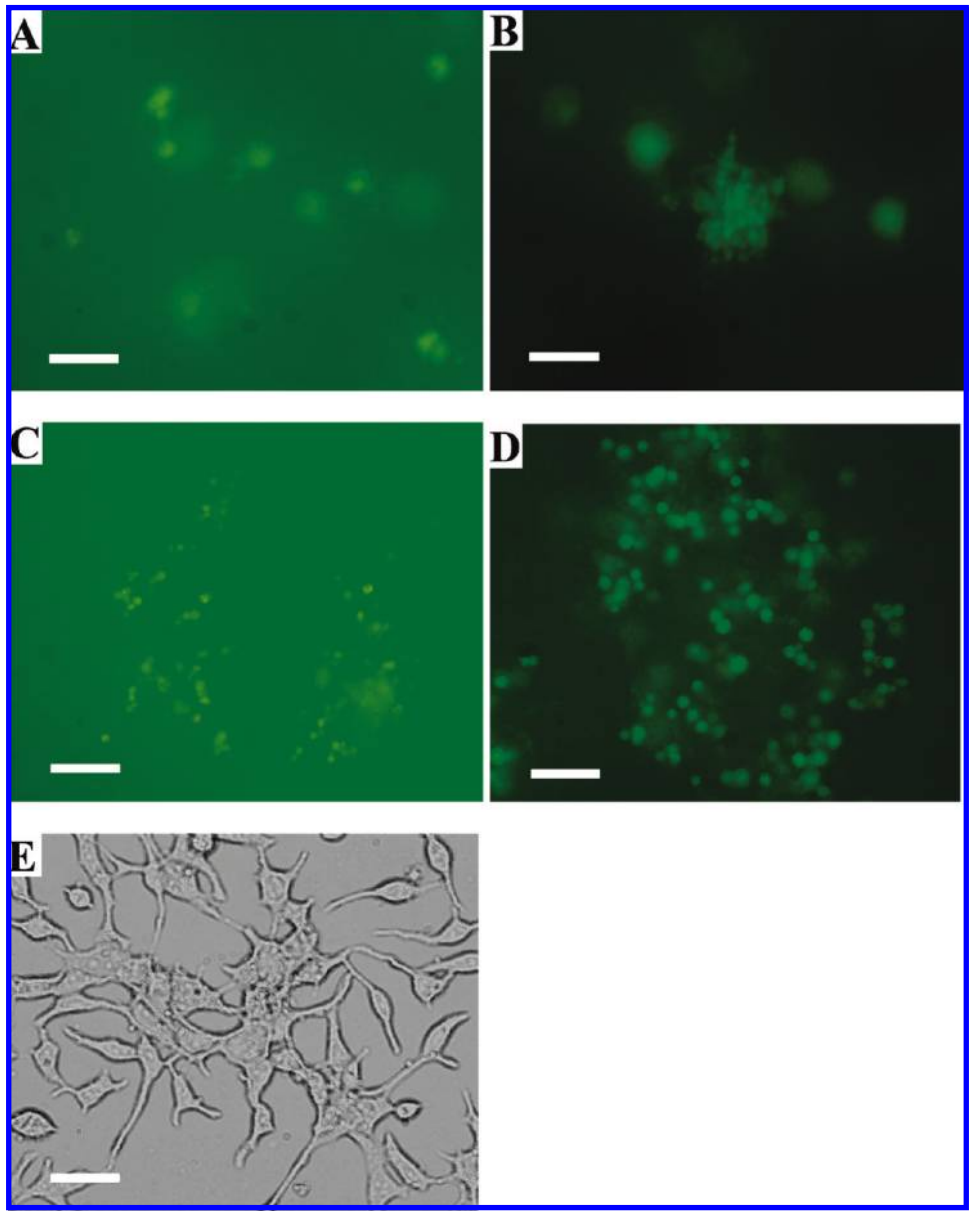

Figure 9. (A−D) Fluorescence images of 293T cells cultured in the in situ formed P(NIPAM-HEMA) microgel scaffold for 3 (A), 6 (B), 12 (C), and 18 days (D). The cells were stained with AO. (E) 293T cells in monolayer culture. Scale bar: 100 μm.

rearrangement of the microgel particles. Quick freezing also avoids the formation of ice crystals, which may also change the microstructure of the hydrogel.

To test the potential of the microgel dispersion as a novel injectable 3D scaffold for cell culture, 293T cells, a human kidney cell line, were mixed with the microgel dispersion at room temperature. Solid cell/matrix construct formed immediately when the mixture was brought to 37 °C. After being cultured for a certain period, the number of viable cells was determined using the colorimetric MTT assay. Viable cells have the cellular reductive capacity to metabolize the yellow water-soluble tetrazolium salt, MTT, to the water-insoluble blue formazan product. So the optical density values in MTT assay represent the actual viable cell numbers. As shown in Figure 8, for the first several days, no significant change in the number of viable cells was observed. Viable cells increases continuously from the 4th day to 16th day, suggesting that the in situ-formed scaffold supports cell proliferation. However, a slight decrease in viable cell number was observed on the 22nd day, probably due to a cell density in the scaffold that was too high. It has been reported that oxygen can be depleted in long-term 3D culture when cell density in the matrix is high.[28,29] These problems can be alleviated in dynamic culture with improved oxygen transfer and continuous media perfusion.

The morphology of cells cultured in the 3D scaffold was studied using inverted fluorescence microscopy after stained with acridine orange (AO). For the first several days, all the cells are round in shape with a diameter of about 20 μm (Figure 9A). This morphology is very different from that of the cells in 2D cultures, which attach on the surface of the culture flask and present a spread, irregular shape with protrusions (Figure 9E). The round cell shape suggests that the cells may not attach with the scaffold. Similar results have been reported by other authors.[30] When cultured for 6 days, small cells with a diameter of only several microns appeared (Figure 9B). From then on, only these small cells were observed, however, the cell density increases gradually with culture time (Figure 9B−D), indicating a continuing cell proliferation, which is in accordance with the previous MTT assay (Figure 8). It is well-known that cells often behave differently in 3D scaffold from that in 2D cultures.[1–3,31,32]

3D scaffolds provide individual cells complex interactions with the immediate neighbors and the artificial extracellular matrices, which may control the cells' behavior but are lost in monolayer 2D cultures. In addition, in 2D cultures, cells are directly exposed to the nutrient- and oxygen-rich media. In contrast, in 3D cultures, nutrient and oxygen are transported through the interconnected pores. The limited supply in nutrient and oxygen may be the main reason for the reduced size of the cells growing in 3D scaffold. The cells cultured for 18 days is somewhat bigger than the cells cultured for 12 days, possibly indicating that the cells adapt their new environment gradually and so grow to a bigger size.

Conclusions

In conclusion, thermosensitive P(NIPAM-HEMA) microgel particles were used as the building blocks to construct injectable thermal gelling scaffold for 3D cell culture. The concentrated microgel dispersion is colloidally stable when heated above its VPTT because the hydrophobic interactions between the shrunk microgel particles are not strong enough to dominate the electrostatic repulsion. However, in the presence of Ca^{2+}, with the introduction of additional ionic cross-linking, macroscopic hydrogel forms as a result of the thermally induced spontaneous gelation. The resultant bulky gels present an interconnected porous microstructure that is highly desirable for their use as 3D scaffold. Preliminary cell culture proved that the in situ-formed hydrogels are biocompatible and support cell proliferation.

Acknowledgment. We thank financial support for this work from the Ministry of Science and Technology of China (Grant No. 2007DFA50760), Tianjin Committee of Science and Technology (07ZCGHHZ01200), and the National Natural Science Foundation of China (Grant No. 20774049).

Supporting Information Available. Figures showing the evolution of dynamic modulus of a 6.0 wt % P(NIPAM-HEMA) microgel dispersion containing 0.154 M NaCl with temperature increase and photographs of 6 wt % P(NIPAM-HEMA) microgel dispersion under various conditions. This material is available free of charge via the Internet at http://pubs.acs.org.

References and Notes

(1) (a) Lee, K. Y.; Mooney, D. J. *Chem. Rev.* **2001**, *101*, 1869–1879. (b) Lee, J.; Cuddihy, M. J.; Kotov, N. A. *Tissue Eng., Part B* **2008**, *14*, 61–86.
(2) Xu, F.; Burg, K. J. L. *Cytotechnology* **2007**, *54*, 135–143.
(3) Cushing, M. C.; Anseth, K. S. *Science* **2007**, *316*, 1133–1134.
(4) Kotov, N. A.; Liu, Y. F.; Wang, S. P.; Cumming, C.; Eghtedari, M.; Vargas, G.; Motamedi, M.; Nichols, J.; Cortiella, J. *Langmuir* **2004**, *20*, 7887–7892.
(5) Hou, Q. P.; De Bank, P. A.; Shakesheff, K. M. *J. Mater. Chem.* **2004**, *14*, 1915–1923.
(6) Ruel-Gariepy, E.; Leroux, J. C. *Eur. J. Pharm. Biopharm.* **2004**, *58*, 409–426.
(7) Jeong, B.; Lee, K. M.; Gutowska, A.; An, Y. H. H. *Biomacromolecules* **2002**, *3*, 865–868.
(8) Nagahama, K.; Ouchi, T.; Ohya, Y. *Adv. Funct. Mater.* **2008**, *18*, 1220–1231.
(9) Yu, L.; Ding, J. D. *Chem. Soc. Rev.* **2008**, *37*, 1473–1481.
(10) Jaklenec, A.; Wan, E.; Murray, M. E.; Mathiowitz, E. *Biomaterials* **2008**, *29*, 185–192.
(11) Stile, R. A.; Burghardt, W. R.; Healy, K. E. *Macromolecules* **1999**, *32*, 7370–7379.
(12) Kim, S.; Healy, K. E. *Biomacromolecules* **2003**, *4*, 1214–1223.
(13) Au, A.; Ha, J.; Polotsky, A.; Krzyminski, K.; Gutowska, A.; Hungerford, D. S.; Frondoza, C. G. *J. Biomed. Mater. Res., Part A* **2003**, *67A*, 1310–1319.
(14) Ibusuki, S.; Fujii, Y.; Iwamoto, Y.; Matsuda, T. *Tissue Eng.* **2003**, *9*, 371–384.
(15) Ohya, S.; Nakayama, Y.; Matsuda, T. *Biomacromolecules* **2001**, *2*, 856–863.
(16) Kidane, A.; Szabocsik, J. M.; Park, K. *Biomaterials* **1998**, *19*, 2051–2055.
(17) Lu, S. X.; Anseth, K. S. *J. Controlled Release* **1999**, *57*, 291–300.
(18) Brugger, B.; Richtering, W. *Adv. Mater.* **2007**, *19*, 2973–2978.
(19) Ma, X. M.; Tang, X. Z. *Acta Polym. Sin.* **2006**, 937–943.
(20) (a) Daly, E.; Saunders, B. R. *Langmuir* **2000**, *16*, 5546–5552. (b) Rasmusson, M.; Routh, A.; Vincent, B. *Langmuir* **2004**, *20*, 3536–3542.
(21) Hu, Z. B.; Xia, X. H. *Adv. Mater.* **2004**, *16*, 305–309.
(22) Benee, L. S.; Snowden, M. J.; Chowdhry, B. Z. *Langmuir* **2002**, *18*, 6025–6030.
(23) Senff, H.; Richtering, W. *J. Chem. Phys.* **1999**, *111*, 1705–1711.
(24) Saunders, B. R.; Vincent, B. *Adv. Colloid Interface Sci.* **1999**, *80*, 1–25.
(25) Kuo, C. K.; Ma, P. X. *Biomaterials* **2001**, *22*, 511–521.
(26) Park, T. G.; Hoffman, A. S. *Macromolecules* **1993**, *26*, 5045–5048.
(27) Xia, X. H.; Tang, S. J.; Lu, X. H.; Hu, Z. B. *Macromolecules* **2003**, *36*, 3695–3698.
(28) Ouyang, A.; Ng, R.; Yang, S. T. *Stem Cells* **2007**, *25*, 447–454.
(29) Volkmer, E.; Drosse, I.; Otto, S.; Stangelmayer, A.; Stengele, M.; Kallukalam, B. C.; Mutschler, W.; Schieker, M. *Tissue Eng., Part A* **2008**, *14*, 1331–1340.
(30) Tae, G.; Kim, Y. J.; Choi, W. I.; Kim, M.; Stayton, P. S.; Hoffman, A. S. *Biomacromolecules* **2007**, *8*, 1979–1986.
(31) Abbott, A. *Nature* **2003**, *424*, 870–872.
(32) Cukierman, E.; Pankov, R.; Stevens, D. R.; Yamada, K. M. *Science* **2001**, *294*, 1708–1712.

BM900022M